Bulletin of the Seismological Society of America, Vol. 93, No. 4, pp. 1835–1840, August 2003

Estimation of the Critical Slip-Weakening Distance: Theoretical Background

by Eiichi Fukuyama, Takeshi Mikumo, and Kim B. Olsen

Abstract It has been shown that a trade-off exists between estimates of the breakdown strength drop and the critical slip-weakening distance (e.g., Guatteri and Spudich, 2000). For this reason, only the fracture energy, proportional to these two parameters, may be estimated from waveform modeling. However, Mikumo *et al.* (2003) proposed a new technique to estimate the slip-weakening distance of earthquakes, separate from the fracture energy. For this method to be valid, the peak slip-velocity time must be close to the stress breakdown time. Here we explain the theoretical background of this assumption and clarify the limitations of this technique using numerical simulations based on the boundary integral equation method. The theoretical analysis using the boundary integral equation and some numerical tests indicates that a rather smooth rupture process and relatively sharp change in stress at the stress breakdown time in the slip-weakening curve ensure the validity of the method.

Introduction

It is quite important to estimate the critical slip-weakening distance (D_c) because it controls the nucleation process of earthquakes (e.g., Matsu'ura *et al.*, 1992) as well as their dynamic rupture history (e.g., Fukuyama and Madariaga, 2000). Critical slip-weakening friction was theoretically proposed by Ida (1972) and Palmar and Rice (1973), and it was measured by Ohnaka *et al.* (1987) in the laboratory. Ohnaka and Shen (1999) proposed a scaling relation in D_c, and Ide and Takeo (1997) estimated D_c from the inversion of strong motion waveforms of the 1995 Kobe earthquake. However, Guatteri and Spudich (2000) claimed that there is a trade-off between D_c and $\Delta\tau_b$ (breakdown strength drop) and insisted that fracture energy (G_c) is the only parameter that controls the dynamic rupture if the high-frequency behavior of fault motion is ignored.

Marone and Kilgore (1993) showed that the critical slip-weakening displacement is related to the thickness of the fault gouge as well as the surface roughness. If we are able to estimate D_c reliably for past earthquakes, we will therefore be able to discuss the relation between earthquake size and thickness of the fault. This might provide us with important information about the earthquake generation process. Recently, Hirose and Shimamoto (2002) proposed from laboratory experiments that the melting due to frictional heating causes a long critical slip-weakening distance during high-speed faulting. The present method might enable us to confirm the hypothesis of longer D_c due to frictional heating from near-fault observations during the earthquake.

Mikumo *et al.* (2003) proposed a method to estimate D_c using slip-rate time functions on the fault. This method assumes that the peak slip-rate time (hereafter we call this time T_{pv}) should be close to the strength breakdown time (T_b). Then D_c can be estimated without measuring the stress behavior. This idea can be easily extended to measure the D_c of an earthquake from near-fault seismograms if the waveforms are well approximated to the slip function on the fault (Olsen *et al.*, unpublished manuscript, 2003).

In this article, we examine the validity of the assumption made by Mikumo *et al.* (2003) from a theoretical point of view. In particular, we demonstrate why the slip velocity attains a maximum close to T_b, the breakdown stress time based on the explicit integral equation. Then, we discuss the effect of fault heterogeneity using a simple fault model. Finally, we compare the results for various shapes of slip-weakening relations using numerical simulations.

Theoretical Background

The key issue of the method proposed by Mikumo *et al.* (2003) for the estimation of D_c by slip-rate functions is that T_{pv} should be close to T_b. In order to theoretically understand the validity of this assumption, we consider a fault in a homogeneous infinite elastic medium.

As a boundary condition on the fault, the following equation can be obtained, as shown in Fukuyama and Madariaga (1998):

$$\boldsymbol{\tau}(\mathbf{x},t) = -\frac{\mu}{2\beta}\,\Delta\dot{\mathbf{u}}(\mathbf{x},t) + \int_S \int_0^t K(\mathbf{x}-\boldsymbol{\xi},\, t-\tau)\Delta\dot{\mathbf{u}}(\boldsymbol{\xi},\tau)d\tau d\boldsymbol{\xi}, \quad (1)$$

where $\boldsymbol{\tau}$ and $\Delta\dot{\mathbf{u}}$ are the stress and slip velocity on the fault, respectively, K is the integration kernel that is the contribution from the past slip history, μ and β are the rigidity and shear-wave velocity, respectively, and S is the ruptured area. A rigorous description of K for a planar crack can be found in Fukuyama and Madariaga (1998). This equation is still valid for a nonplanar fault by using an appropriate K for nonplanar faults (Tada *et al.*, 2000). It should be noted that this equation is universal and valid as far as the crack is sufficiently thin because the only assumption for this equation is the continuity and discontinuity of stress and displacement on the crack surface and elasticity outside the crack. Thus it should also be emphasized that this equation is independent of the constitutive law on the fault.

In equation (1), the second term on the right-hand side represents the stress change due to the past slip. If this term behaves smoothly around T_{pv}, the total stress ($\boldsymbol{\tau}$) should change abruptly around T_{pv}, because in this case stress is almost proportional to the current slip velocity. Since the integration term represents the stress disturbance due to the elastic waves emitted from the past slip on the fault, we expect that as far as the rupture propagates smoothly, this integration term behaves smoothly.

In Figure 1, an example of this behavior is shown for homogeneous initial stress and strength distribution with a linear slip-weakening relation as idealized by Andrews (1976a,b). This computation was done using Fukuyama and Madariaga's (1998) boundary integral equation code. When the stress drops to the frictional level around T_b, the integration term in equation (1) behaves smoothly, as expected. Thus, in order to satisfy the boundary condition on the fault as in equation (1), the slip velocity should change abruptly and form a local maximum. This is the main reason why T_b is close to T_{pv}. However, near the edge of the fault or near the asperity/barrier where the rupture velocity accelerates or decelerates abruptly, the change of this integration term cannot be ignored. In this case, a stopping phase will be generated and contaminate this relation so that T_{pv} may deviate significantly from T_b. We will examine this situation numerically in detail in the next section.

Effects of Fault Heterogeneity

In order to demonstrate the effects of fault heterogeneity, we simulated a rupture propagation in a fault model with a barrier (high strength patch) and an asperity (high stress patch) as shown in Figure 2a. In this simulation, the initial stress is assumed to be homogeneous (2.2 MPa) except for the asperity patch (2.9 MPa) and initiation part (4.0 MPa). In the barrier patch, the fault strength is raised to 10 MPa from a level of 3.0 MPa on the remaining part of the fault.

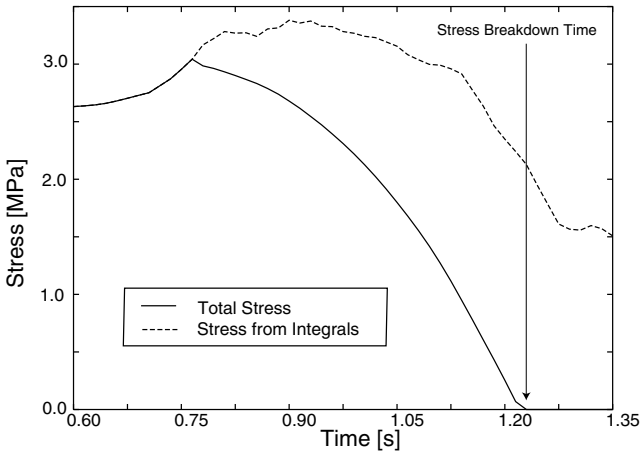

Figure 1. Typical time evolution of the total stress (solid line) and the stress contribution from the integration term (broken line) for a uniform stress drop of 3.5 MPa and D_c of 0.75 m. The fault dimensions are 25.6 km × 12.8 km with a grid size of 0.2 km × 0.2 km and time increment of 0.015 sec.

A linear slip-weakening relation is assumed with a critical slip-weakening distance of 0.8 m. All computations are done by the boundary integral equation method (Fukuyama and Madariaga, 1998).

Snapshots of this simulation are shown in Figure 2b. From this figure, one can see that rupture is accelerated by the asperity and decelerated by the barrier. In the third snapshot (the third row of Fig. 2b), the rupture front has reached the asperity region where stress is raised (horizontal yellow band in the stress plot in Fig. 2b). At the same time, the rupture front has arrived at the barrier region (vertical red band in stress plot in Fig. 2b). After this time, rupture is accelerated downward and is prevented from propagating to the left. In the eighth snapshot the rupture finally overcomes the barrier and has started to propagate again at the lower bottom region where both the asperity band and barrier band are intersected. Then the entire barrier breaks and the whole region ruptures.

In Figure 2c, time histories of stress, slip, and slip rate as well as the stress contribution from the integration term (stress_int) are shown. The four panels correspond to (1) the left and (2) the right of the barrier, and (3) above and (4) below the asperity, respectively. In cases 1, 3, and 4, T_{pv} is close to T_b. However, to the right of the barrier (case 2), where the rupture has stopped at the barrier for a while, T_{pv}

Figure 2. (a) Initial stress and strength distribution for the stress/strength heterogeneity tests. Fault dimensions are 64 km × 64 km. Green and pink meshes represent strength and initial stress, respectively. (b) Snapshots of the dynamic rupture for stress (left column), slip rate (center), and slip (right) at an interval of 0.8 sec. (c) Time functions of slip (pink), slip rate (navy), stress (red), and stress contribution from integrals (green). The locations are shown at upper left panel in (b).

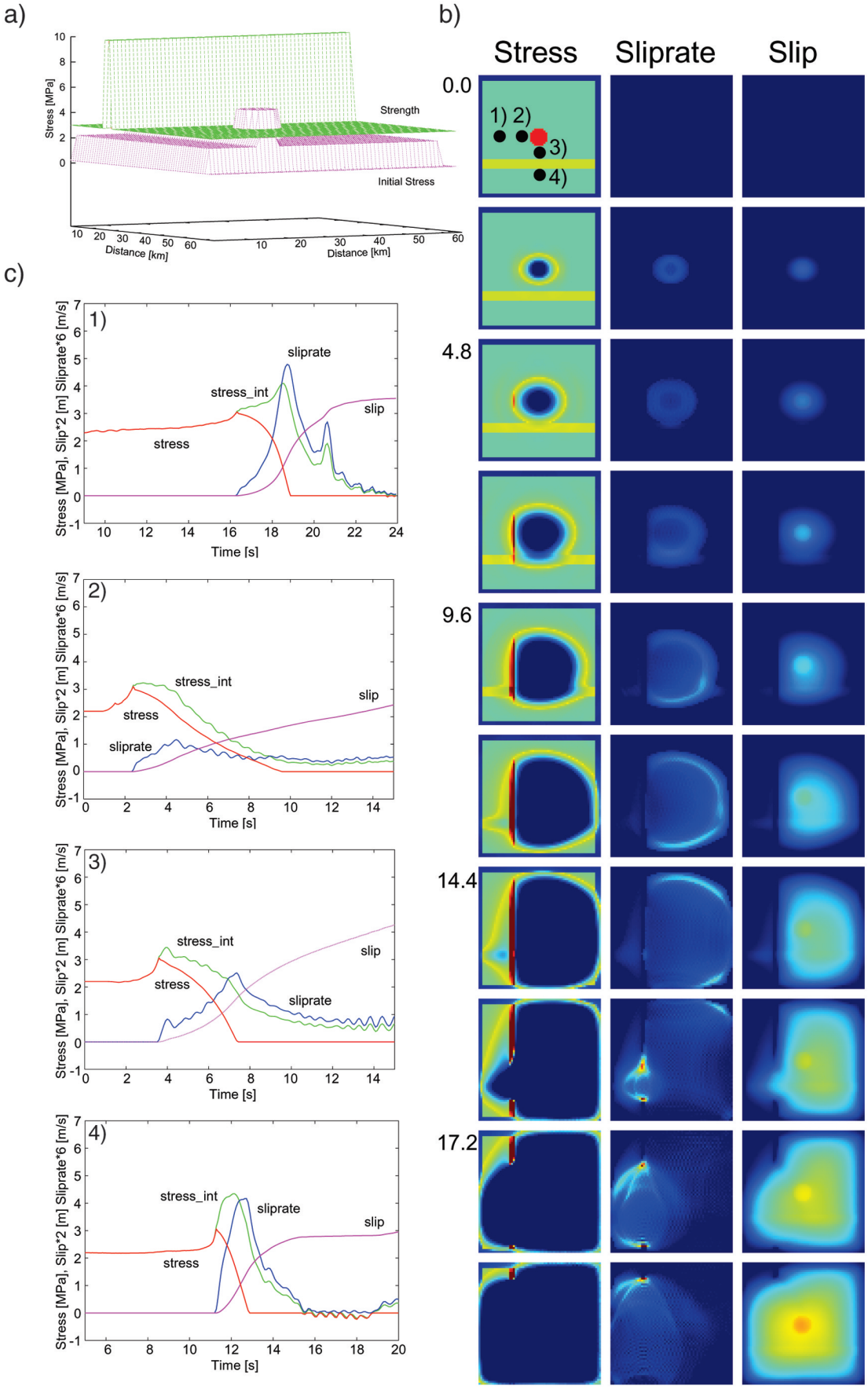
a)
Stress [MPa]
Strength
Initial Stress
Distance [km]
Distance [km]
b)
Stress
Sliprate
Slip
0.0
1) 2)
3)
4)
4.8
9.6
14.4
17.2
c)
1)
2)
3)
4)
Stress [MPa], Slip*2 [m] Sliprate*6 [m/s]
Time [s]
sliprate
stress_int
slip
stress

is significantly earlier than T_b. This is due to the effect of a stopping phase, affecting the stress change of the integration term. On the other hand, the effect of the asperity seems to be small due to a relatively small velocity change. The asperity is oriented along the antiplane rupture direction so that the maximum rupture velocity is the shear-wave velocity.

Thus our results indicate that if the rupture velocity does not change abruptly, the method for estimating D_c by Mikumo *et al.* (2003) will work properly. However, if the rupture velocity changes abruptly due to the existence of a barrier, for example, the method might not work correctly.

Effect of the Shape of the Slip-Weakening Curve

In this section we examine the sensitivity of our method for estimating D_c with respect to the shape of the slip-

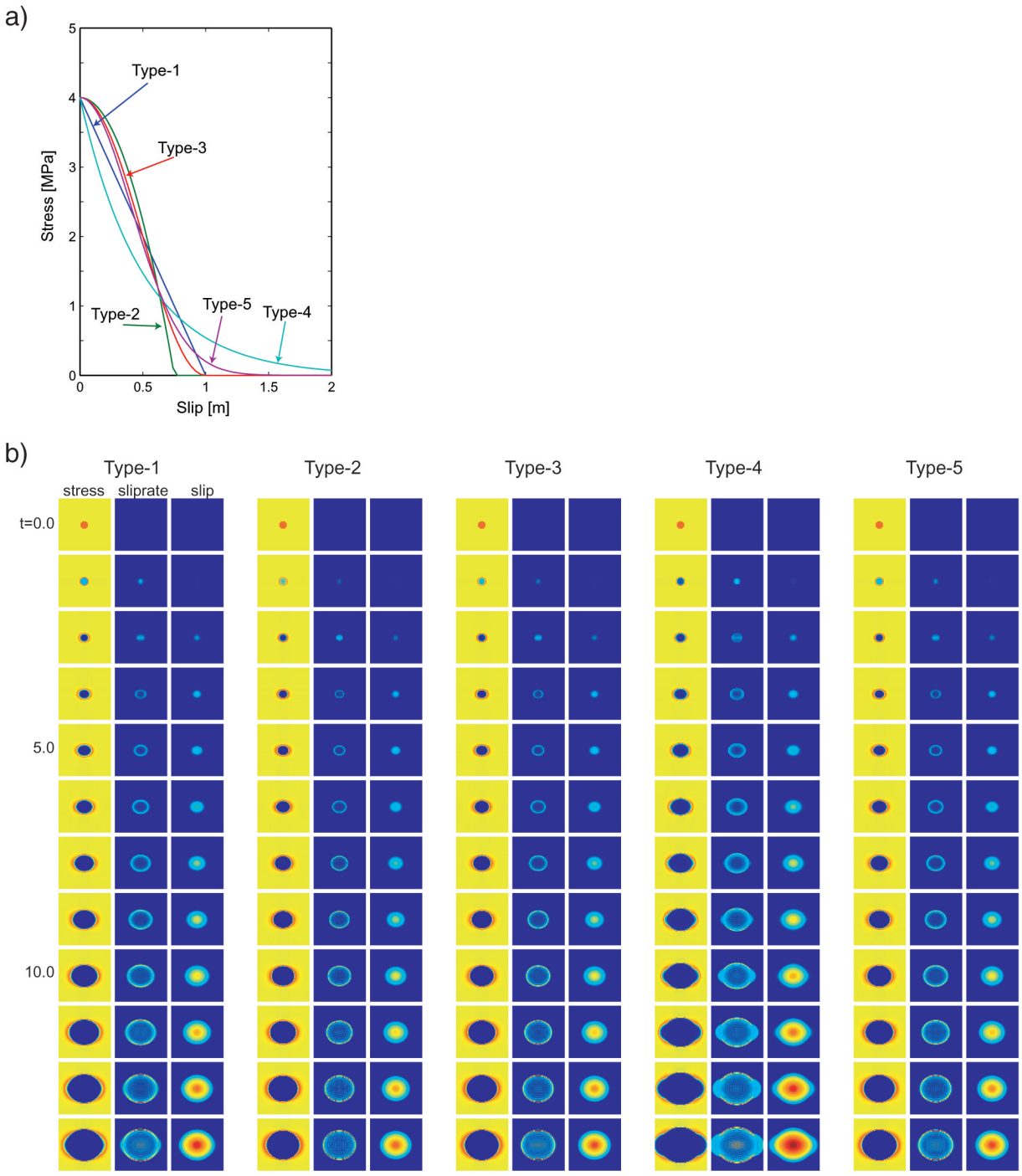

Figure 3. (a) Shapes of slip-weakening functions used in the slip-weakening shape test. (b) Snapshots of resultant dynamic ruptures at an interval of 0.8 sec for five different slip-weakening curves shown in (a). Fault dimensions are 64 km × 64 km.

weakening curve. We consider five types of slip-weakening laws as shown in Figure 3a. Type 1, type 2, and types 3–5 correspond approximately to those used in Andrews (1976a,b), Campillo *et al.* (2001), and Matsu'ura *et al.* (1992), respectively. Each function is mathematically described in Table 1. For types 1, 3, and 5 we set D_c to 1 m, for type 2 to 0.75 m, and for type 4 to 1.5 m in order to keep G_c the same among the five friction laws. As shown in Fukuyama and Olsen (2002), if G_c is kept constant, the rupture histories become similar to each other under the same initial stress. As shown in the previous section, in order to estimate D_c correctly from T_{pv}, an abrupt change in stress is required when slip reaches D_c. Type 2 changes the stress most rapidly around D_c and type 4 most smoothly, while the behavior of types 1, 3, and 5 are in between those of types 2 and 4. All the computations are done under the same homogeneous initial stress condition.

In Figure 3b, snapshots of stress, slip rate, and slip for each slip-weakening model are shown. These snapshots are quite similar, as expected. The snapshots of type 4 are slightly different from the others. This is due to the long tail in the slip-weakening curve, which makes G_c a bit smaller. However, this difference is quite minor, as discussed in Fukuyama and Madariaga (2000).

In Figure 4a, the spatial distribution of the estimation error $D'_c - D_c$ is shown for slip-weakening types 1–5, where D_c is the slip-weakening distance assumed for each curve and D'_c is the apparent slip-weakening distance estimated from the peak slip-rate time T_{pv}. From these figures the estimation error is the smallest in type 2 and the largest for type 4. In all cases, D_c is estimated better along the in-plane direction than the anti-plane direction. Figure 4b shows the histograms of the estimation error $D'_c - D_c$. It should be noted that the true D_c are set to be 1.0, 0.75, 1.0, 1.5, and 1.0 m for types 1–5, respectively, in order to keep G_c constant. Thus the mean values and their standard deviations shown in Figure 4b should be treated as relative values, that is, all values should be normalized by D_c in order to avoid the effect of D_c. From these figures, we observe that the $D'_c - D_c$ values are systematically shifted toward negative values. This is because D'_c tends to be underestimated when the slip-weakening curve is gentle at T_b. And this situation can easily occur for type 4, for example. The mean estimation errors for types 1 and 2 are about 3.5% and 0.1%, respectively. For these cases the method works very well with sufficient accuracy. However, for types 3 and 5, the mean errors exceed 20% and for type 4 they reach about 50%. The standard deviations of the estimation error are less than 20% for types 1–3 and 5, but exceed 30% for type 4. Thus we have shown that the dependence of the slip-weakening function is critical for our method to estimate D_c accurately. D_c can be estimated with sufficient accuracy for types 1–3 and 5, but may not be for type 4.

Table 1
Mathematical Formulation of Slip-Weakening Friction Laws used in the Present Study

Name	Mathematical Formulation
Type 1	$\tau = \begin{cases} -\Delta\tau_b/D_c\ \Delta u + \sigma_c & (\Delta u < D_c) \\ \sigma_f & (\Delta u \geq D_c) \end{cases}$
Type 2	$\tau = \begin{cases} -\Delta\tau_b/D_c^2\ \Delta u^2 + \sigma_c & (\Delta u < D_c) \\ \sigma_f & (\Delta u \geq D_c) \end{cases}$
Type 3	$\tau = \begin{cases} \Delta\tau_b/2\ \cos(\pi/D_c\ \Delta u) + (\sigma_c + \sigma_f)/2 & (\Delta u < D_c) \\ \sigma_f & (\Delta u \geq D_c) \end{cases}$
Type 4	$\tau = \Delta\tau_b \exp(-3/D_c\ \Delta u) + \sigma_f$
Type 5	$\tau = \Delta\tau_b \exp(-3/D_c^2\ \Delta u^2) + \sigma_f$

τ and d represent shear stress and slip on the fault. $\Delta\tau_b$ is the breakdown strength drop ($\sigma_c - \sigma_f$); σ_c and σ_f stand for critical stress and frictional stress, respectively.

Conclusions

We have demonstrated the theoretical background of the method of Mikumo *et al.* (2003) for the estimation of the slip-weakening distance from the slip and slip-rate functions, independent of the fracture energy. We show that this method works well if the source process is relatively smooth, that is, where the stopping phase is not dominant, as well as if the slip-weakening relation changes sharply at the stress breakdown time. These two conditions seem essential when applying the method proposed by Mikumo *et al.* (2003). The most important application might be to estimate the D_c from the near-fault strong motion waveforms, which is work in progress by Olsen *et al.* (unpublished manuscript, 2003).

References

Andrews, D. J. (1976a). Rupture propagation with finite stress in antiplane strain, *J. Geophys. Res.* **81,** 3575–3582.

Andrews, D. J. (1976b). Rupture velocity of plane strain shear crack, *J. Geophys. Res.* **81,** 5679–5687.

Campillo, M., P. Favreau, I. R. Inoescu, and C. Voisin (2001). On the effective friction law of a heterogeneous fault, *J. Geophys. Res.* **106,** 16,307–16,322.

Fukuyama, E., and R. Madariaga (1998). Rupture dynamics of a planar fault in a 3D elastic medium: rate- and slip-weakening friction, *Bull. Seism. Soc. Am.* **88,** 1–17.

Fukuyama, E., and R. Madariaga (2000). Dynamic propagation and interaction of a rupture front on a planar fault, *Pure Appl. Geophys.* **157,** 1959–1979.

Fukuyama, E., and K. B. Olsen (2002). A condition for super-shear rupture propagation in a heterogeneous stress field, *Pure Appl. Geophys.* **159,** 2047–2056.

Guatteri, M., and P. Spudich (2000). What can strong motion data tell us about slip-weakening fault-friction law? *Bull. Seismol. Soc. Am.* **90,** 98–116.

Hirose, T., and T. Shimamoto (2002). Weakening mechanism of faults

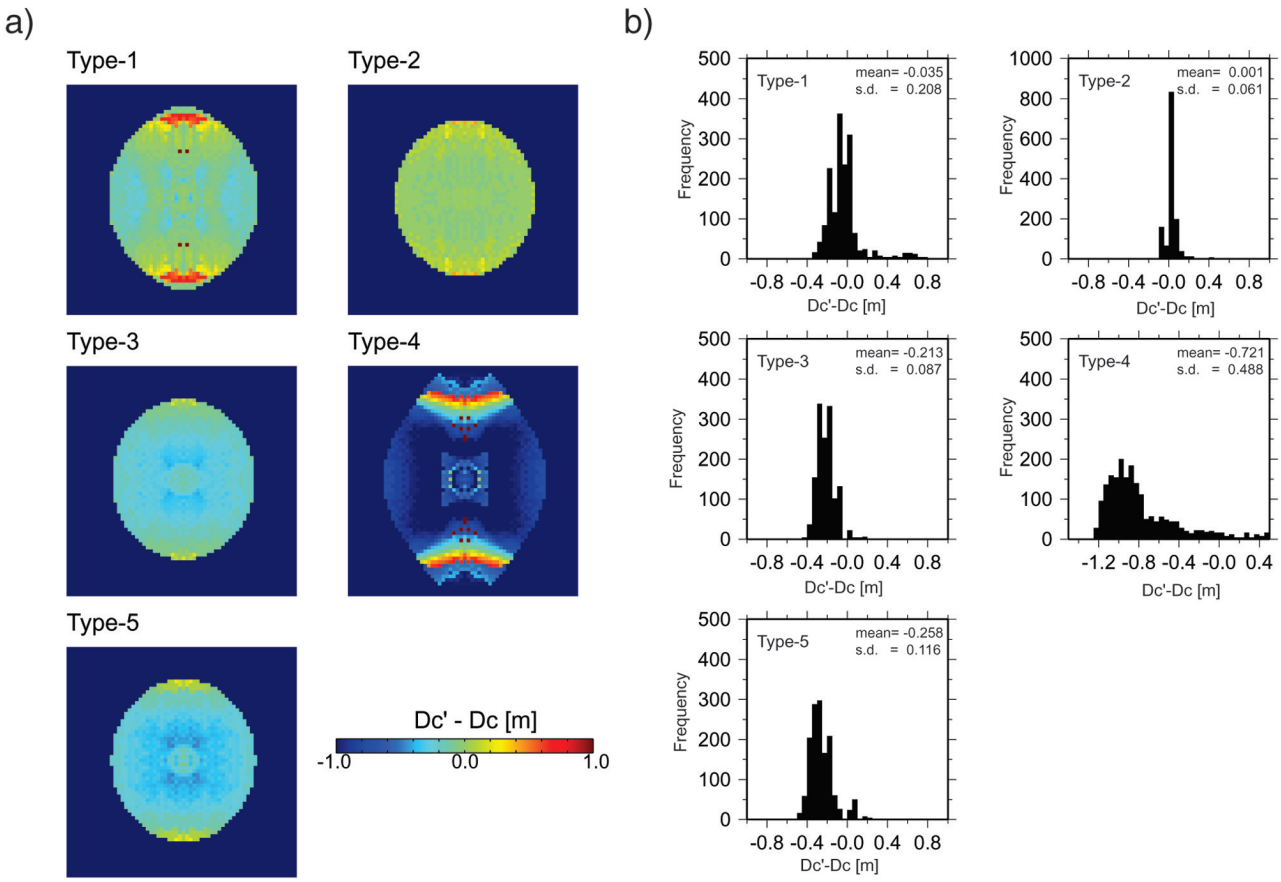

Figure 4. (a) Distributions of $D_c' - D_c$ for five different slip-weakening curves. The area smaller than -1.0 is the region where slip did not reach the slip-weakening distance. (b) Frequency distribution of $D_c' - D_c$. Mean values and standard deviations are listed at upper right of each panel.

during frictional melting, *Abstracts 2002 Japan Earth and Planetary Science Joint Meeting*, G061-0004, the Japan Earth and Planetary Science Joint Meeting Organization, Tokyo, 26–29 May (CD-ROM).

Ida, Y. (1972). Cohesive force across the tip of a longitudinal—shear crack and Griffith's specific surface energy, *J. Geophys. Res.* **77,** 3796–3805.

Ide, S., and M. Takeo (1997). Determination of constitutive relations of fault slip based on seismic wave analysis, *J. Geophys. Res.* **102,** 27,379–27,391.

Marone, C., and B. Kilgore (1993). Scaling of the critical slip distance for seismic faulting with shear strain in fault zones, *Nature* **362,** 618–621.

Matsu'ura, M., H. Kataoka, and B. Shibazaki (1992). Slip dependent friction law and nucleation processes in earthquake rupture, *Tectonophysics* **211,** 135–142.

Mikumo, T., K. B. Olsen, E. Fukuyama, and Y. Yagi (2002). Stress-breakdown time and slip-weakening distance inferred from slip-velocity functions on earthquake faults, *Bull. Seism. Soc. Am.* **93,** 264–282.

Ohnaka, M., and L.-F. Shen (1999). Scaling of the shear rupture process from nucleation to dynamic propagation: implications of geometric irregularity of the rupturing surfaces, *J. Geophys. Res.* **104,** 817–844.

Ohnaka, M., Y. Kuwahara, and K. Yamamoto (1987). Constitutive relations of dynamic physical parameters near a tip of the propagating slip zone during stick-slip shear failure, *Tectonophysics* **175,** 197–220.

Palmer, A. C., and J. R. Rice (1973). The growth of slip surfaces in the progressive failure of over-consolidated clay, *Proc. R. Soc. London A* **332,** 527–548.

Tada, T., E. Fukuyama, and R. Madariaga (2000). Non-hypersingular boundary integral equations for 3D nonplanar crack dynamics, *Comp. Mech.* **25,** 613–626.

National Research Institute for Earth Science and Disaster Prevention
Tsukuba, Ibaraki, 305-0006, Japan
fuku@bosai.go.jp
(E.F.)

Instituto de Geofisica, Universidad Nacional Autonoma de Mexico
Mexico 04510 D.F., Mexico
mikumo@ollin.igeofcu.unam.mx
(T.M.)

Institute for Crustal Studies
University of California, Santa Barbara
Santa Barbara, California 93106
kbolsen@crustal.ucsb.edu
(K.B.O.)

Manuscript received 22 August 2002.